Characterizing the cellular architecture of the tumor microenvironment using imaging mass cytometry and digital image analysis with the HALO® and HALO AI platform

Introduction

The tumor microenvironment (TME) is the seat of multiple cell interactions, including those between tumor cells, immune cells, stromal cells, and others. The identification of the markers expressed, and their spatial distribution can help not only to establish a prognosis of the disease, but also to direct therapeutic selection.[1] Imaging mass cytometry™ (IMC™), which uses antibodies conjugated to metal tags, allows for the simultaneous evaluation of the expression of more than 40 protein biomarkers while investigating cellular and histological context.[2] Through mass tagging, IMC also avoids issues that can complicate fluorescent imaging, including autofluorescence, spectral bleed-through, and the need to rigidly order antibody introduction.

In this application note, we describe how the HALO® Highplex FL module and HALO AI can be used in a convenient workflow for analysis of the TME and highly multiplexed IMC images. The Highplex FL module is capable of processing unlimited channels and user-defined phenotypes of biomarkers localized to membrane, cytoplasmic, and nuclear compartments. HALO AI is a set of train-by-example tools for segmentation, classification, and phenotyping that leverages deep learning neural networks. With HALO AI, classifiers can be trained to quantify tissue classes, segment nuclei and/or tissue classes for analysis with other HALO modules, find rare events or cells, and categorize cell populations into specific phenotypes. Leveraging these capabilities, we demonstrate how AI-based image analysis tools allow for identification of tumor cells irrespective of differentially expressed biomarkers and increase spatial analysis sensitivity and reproducibility by aiding detection and annotation of tissues.

Image Acquisition and Analysis Workflow

Tumor types studied in this application note included ovarian adenocarcinoma, low- and high-grade urothelial carcinoma, lung adenocarcinoma, esophageal squamous cell carcinoma, pancreatic ductal adenocarcinoma, and gastric adenocarcinoma. IMC images were collected on the Hyperion Imaging System by Standard BioTools, and the biomarkers analyzed included alpha SMA, vimentin, pan-CK, PD-L1, FoxP3, CD4, E-cadherin, CD68, CD20, CD8a, PD-1, granzyme B, Ki67, collagen, CD3, PHH3, and CD45RO. Images were kindly provided by Standard BioTools as OME-TIFF for subsequent analysis with HALO.

The image analysis workflow for this study of the TME

Figure 1. Image analysis workflow. **A**. Pattern-based nuclear segmentation network. **B**. Nuclear phenotyper network for tumor (blue), stromal (magenta), and immune (yellow) cell identification. **C**. Pattern-based tissue classification of the tumor (blue) and stroma (magenta). **D**. Biomarker evaluation based on positivity thresholding. **E**. Spatial analysis of the TME (colors denote 100 µm bands inside/outside tumor margin).

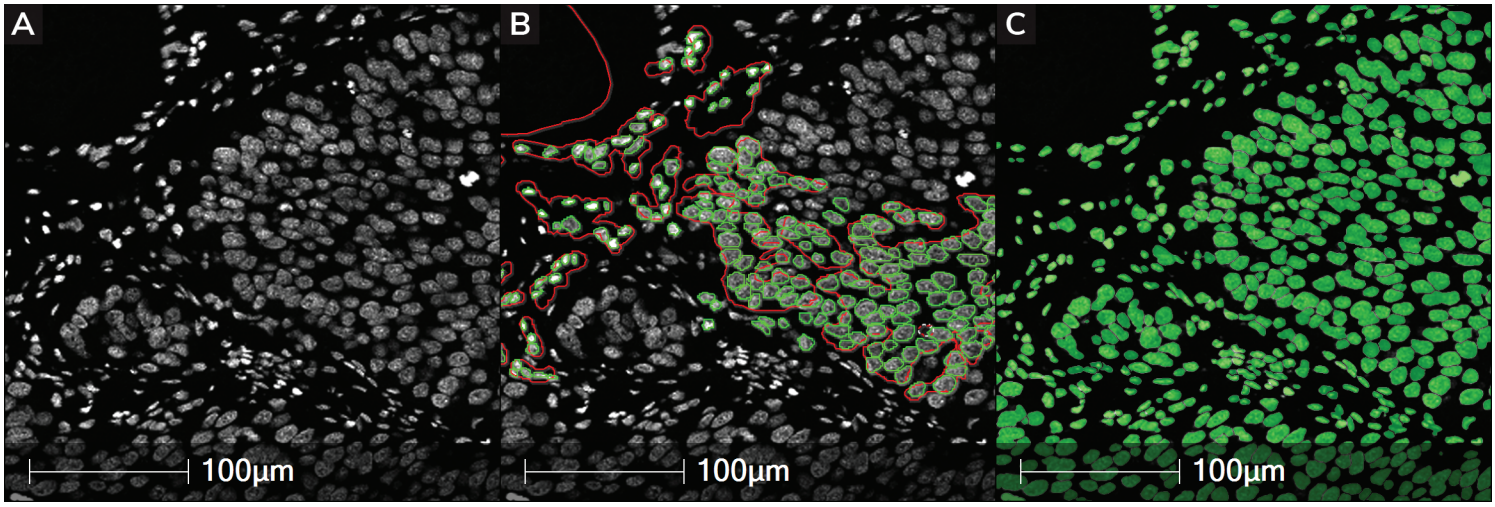

Figure 2. HALO AI nuclear segmentation. **A**. DNA channels of a high-grade urothelial carcinoma IMC image. **B**. Representative annotations of nuclei (green) and background regions (red) used for HALO AI nuclei segmentation algorithm training. **C**. Nuclei (green) segmented using trained algorithm.

is represented in **Figure 1** and began with the training of three pattern-based networks within HALO AI. Together, these networks provide increased analytic sensitivity, robustness, and ease-of-use. First, to create a single, highly effective nuclear segmentation network across the different cancer types studied, HALO AI's pretrained nuclear segmentation network was further trained (**Figure 1A**). Nuclei from IMC images of ovarian adenocarcinoma, pancreatic ductal adenocarcinoma, rectal adenocarcinoma, prostatic adenocarcinoma, and urothelial carcinoma were included in the additional segmentation network training, which continued for 27,800 iterations.

An AI nuclear phenotyper network, which automatically assigns a phenotype to cells based on example nuclei and defined phenotypes provided by the user, was created to automatically identify tumor, stromal, and immune cells. This network was based off the DNA channels in low- and high-grade urothelial carcinoma, prostatic adenocarcinoma, lung adenocarcinoma, esophageal squamous cell carcinoma, gallbladder adenocarcinoma, and gastric adenocarcinoma images (**Figure 1B**). The network was trained until reaching stable and robust performance at 22,725 iterations. Relying on morphology as opposed to biomarkers allowed us to create a classifier which identified tumor cells irrespective of the differentially expressed markers.

The final network, an AI tissue classifier, was built using the HALO AI DenseNet V2 network to create a robust, automated classifier to track the location of immune cells in relation to the tumor boundary (**Figure 1C**). To capture the variability present in the studied images, the network was trained on diverse stromal and tumoral regions of gallbladder adenocarcinoma, low- and high-grade urothelial carcinoma, esophageal squamous cell carcinoma, and lung adenocarcinoma samples for 6,175 iterations.

The developed AI networks were embedded in the HALO Highplex FL module for various analyses included in this study. Immune cells were identified within this module using positivity thresholding for various biomarkers (**Figure 1D**). The coordinates of the individual cells were used for subsequent spatial analysis to evaluate immune cell density and tumor infiltration (**Figure 1E**).

Nuclear Segmentation with HALO AI

Accurate nuclear detection and segmentation are necessary for valid cellular characterization, yet various cellular and tissue characteristics, including high cell density and irregular nucleus size, shape, and staining, can complicate this foundational image analysis step. As demonstrated in **Figure 2**, after training on representative nuclei across tumor samples (**Figure 2A, B**) the developed nuclear segmentation network

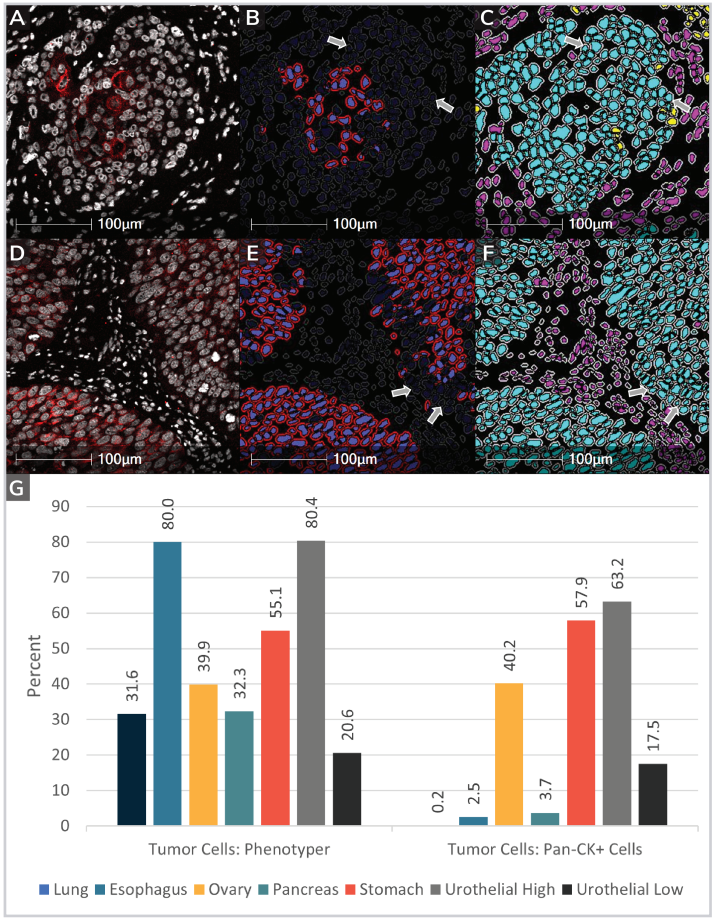

Figure 3. AI phenotyping with DNA channels. **A**. DNA in white and pan-CK in red are shown in esophageal squamous cell carcinoma and **D** high-grade urothelial carcinoma. **B, E**. Highplex FL shows positivity for extranuclear pan-CK in red. Grey arrows point to regions negative for pan-CK but that contain tumor cells according to AI nuclear phenotyper. **C, F**. AI nuclear phenotyper mark-up shows tumor cells in teal, stromal cells in magenta, and immune cells in yellow. Grey arrows as in previous panels. **G**. The percentage of tumor cells identified by the phenotyper (left) or pan-CK positivity (right) was calculated from the total cell count across whole slide images.

exhibited robust performance across the diverse cell types featured in the study (**Figure 2C**). This network was subsequently used throughout the study for nuclear segmentation.

Comparison of Tumor Phenotyping Using AI and Pan-CK Signal Thresholding

Various factors, including suboptimal or variable staining, can complicate the utilization of biomarkers to define cell types. Pan-cytokeratin (pan-CK) positivity has long been the gold standard in cancer research for defining epithelial neoplasms and is commonly utilized in surgical pathology to determine epithelial origin of tissue or to detect metastases in lymph nodes.[3] Defining cell types using biomarker thresholds, such as pan-CK positivity, provides users a readily interpreted visual input, rapid implementation, and easy validation in common protocols. However, biomarker thresholding is susceptible to interobserver variability[4] and sensitive to differences in sample preparation.[5, 6]

As an alternative to biomarker thresholding, AI-enabled nuclear phenotyping provides a biomarker-independent method for enumeration of cells based on morphology alone, is robust to variability in sample preparation, and interpretation is not subject to interobserver variability. Importantly, this approach can be used to enumerate cancer cells undergoing epithelial-to-mesenchymal transition or that otherwise do not express pan-CK.

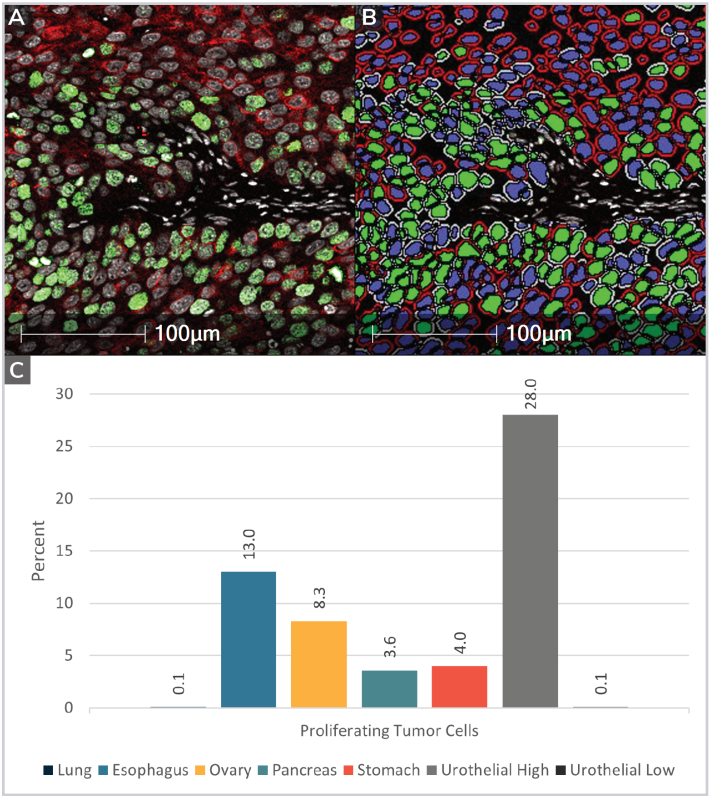

Figure 4. Biomarker quantification in tumor cells. **A**. DNA in white, pan-CK in red, and Ki67 in green are shown in high-grade urothelial carcinoma. **B**. Highplex FL markup in high-grade urothelial carcinoma shows colocalization for tumor cells phenotyped with AI in blue, cytoplasm positivity for Pan-CK in red, and nuclear positivity for Ki67 in green. **C**. Quantification of proliferating tumor cells identified by Ki67 positivity and AI nuclear phenotyping.

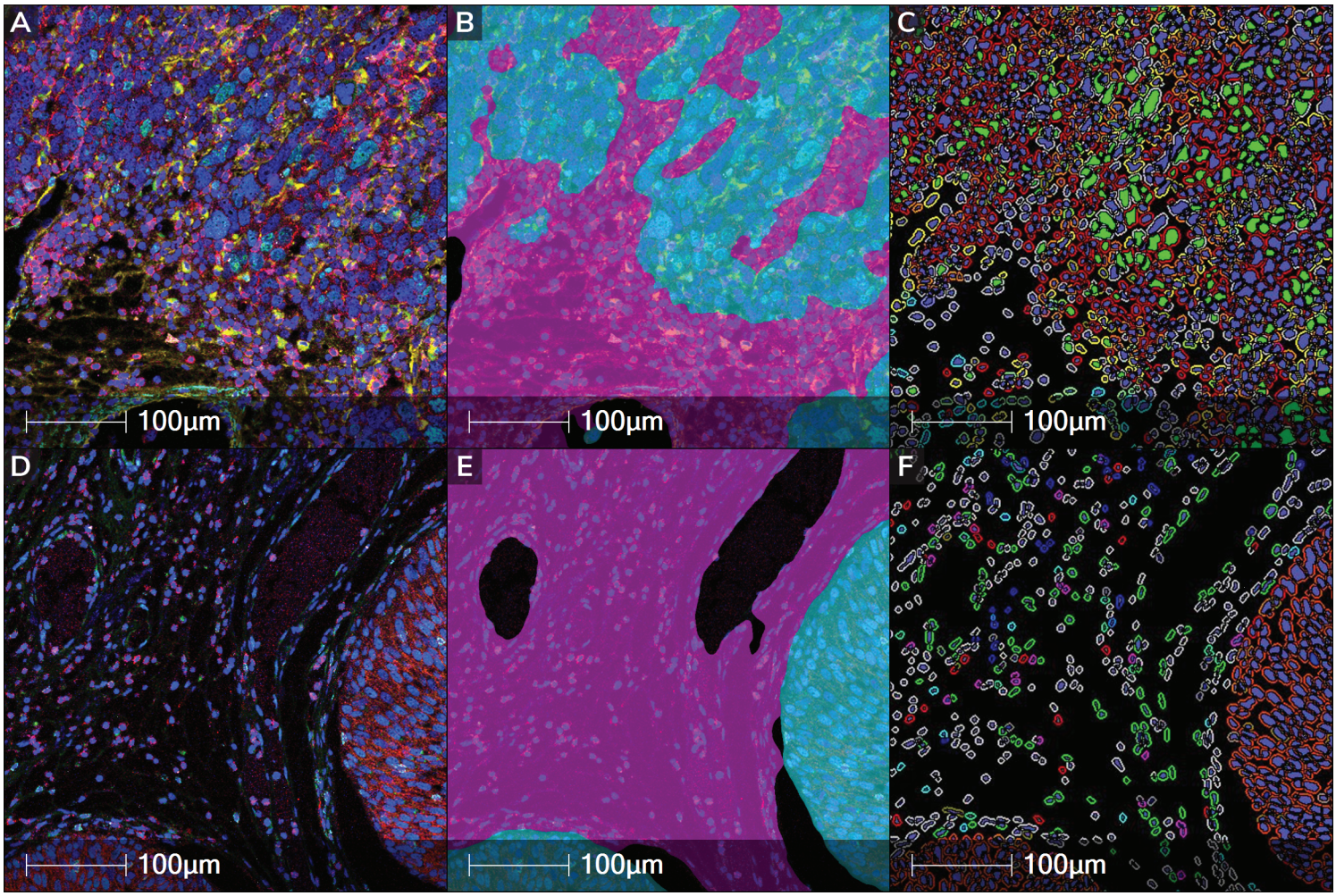

Figure 5. Segmentation and analysis of TME tissue compartments. **A**. All channels are shown in ovarian adenocarcinoma and **D** low-grade urothelial carcinoma. **B, E**. Tumor and stroma AI segmentation is shown in teal and magenta respectively. **C, F**. Highplex FL colocalization analysis of nuclear and cytoplasmic expression for 11 different biomarkers.

Nuclear phenotyping is also commonly used with datasets that feature a diversity of tissue types or sample preparations, including differences in processing date, lab, antibodies, or incubation, or when studies include multiple image analysts. Drawbacks to nuclear phenotyping include subjectivity in the selection of training data and challenges in validating results. Individuals should consider the nature and goals of their study to determine the optimal phenotyping approach for their application.

Though our panel included pan-CK, to demonstrate the capability of the HALO AI nuclear phenotyper to automatically detect cancer cells we compared the percentage of tumor cells identified by the network to the percentage detected by thresholding of pan-CK signal (**Figure 3**). As shown in **Figure 3A-F** and quantified in **Figure 3G**, the degree of agreement between the percentage of cells identified as tumorous by AI phenotyper or pan-CK staining varied between tumor types. In lung, esophagus, and pancreas samples, the AI nuclear phenotyper exhibited higher quantification of tumor cells compared to pan-CK staining, whereas the methodologies showed similar results when identifying ovarian, gastric, and urothelial tumor cells. We hypothesize that a combination of variable cytokeratin biomarker staining and expression changes during epithelial-to-mesenchymal transition were responsible for the differences between the methodologies, though we did not explore the root cause in the current study.

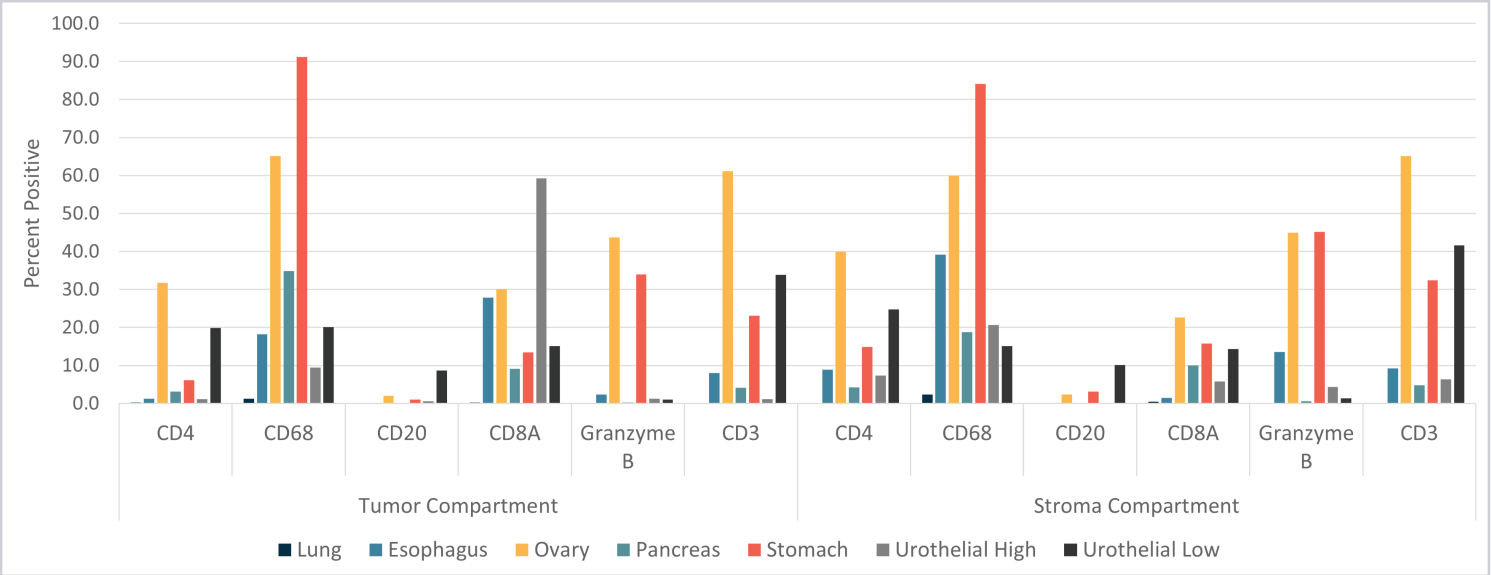

Figure 6. Immune marker quantification of the TME. Biomarker percentage positivity was calculated from total cell count across tumor and stroma compartments in different cancer types.

Biomarker Quantification in Tumor Cells

The AI nuclei phenotyper network was next embedded in the Highplex FL module for TME analysis combining AI-based cell classification and biomarker thresholding (**Figure 4B**). Using AI phenotyping to identify tumor cells and Ki67 biomarker positivity to define proliferative cells, the percentage of proliferating tumor cells was quantified across seven cancer samples (**Figure 4C**). This analysis shows a marked difference in the prevalence of replicating tumor cells across the samples, with this population constituting 28 percent of cells in the high-grade urothelial carcinoma sample but less than one percent of cells in the low-grade urothelial carcinoma and lung adenocarcinoma samples.

Immune Marker Quantification of the TME

In-depth analysis of the TME cellular architecture requires exact annotation of tissue compartments as well as analysis of multiple biomarkers. We leveraged our third AI network to meet this challenge, embedding a HALO AI DenseNet V2 tissue classifier into the Highplex FL module to allow for specific, automatic compartment detection and a streamlined multiplex image analysis workflow (**Figure 5**). Biomarker thresholds were set within Highplex FL and stromal and tumoral compartments were automatically classified by the tissue classifier.

Highplex FL and the embedded tissue classifier were subsequently used to analyze the percentage of biomarker positivity between stromal and tumoral compartments across cancer types (**Figure 6**). Percentage positivity for a given protein was highly heterogeneous between cancer samples, while biomarker prevalence also frequently varied widely between tumor and stroma within a given sample. For example, in the high-grade urothelial carcinoma sample nearly 60 percent of cells in the tumor compartment were CD8A positive while less than 6 percent of cells in the stroma were positive. Comparing CD8A positivity across samples, no other sample exhibited CD8A positivity in more than 31 percent of cells in either compartment.

Density Heatmap of Macrophages

Spatial analyses can provide insight into cellular interactions within the TME, including immune cell modulation of tumor cells, which can be vitally important in predicting cancer progression and response to therapies.[1] The HALO Spatial Analysis module provides a suite of tools to explore spatial relationships between cell populations. The possible analyses include nearest neighbor, which measures the average distance and number of unique neighbors between populations; proximity and infiltration, for determining the number of cells within a defined distance of another cell type or

annotated region, respectively; and density heatmap, which measures the density of members of a cell population within a certain radius. Density heatmapping can be used to identify "hot spots," areas where specific cell phenotypes are more densely populated, in tissues.

Tumor-associated macrophages have been shown to be prognostically important in some tumor types;[1] therefore the Spatial Analysis module was first employed to quantify and visualize CD68+ macrophages across tissues. Using cell data generated from Highplex FL with embedded AI networks, density heatmap analysis was performed within a 25 µm radius of every pixel within the image to plot CD68+ density (**Figure 7A-D**). The tissue classifier network was utilized to measure macrophage density in both stroma and tumor (**Figure 7E**). Varying distributions of macrophages were observed between cancer types; for example, cell hotspots were observed to localize to the stroma in low-grade urothelial carcinoma and distribute throughout the tumor in ovarian adenocarcinoma.

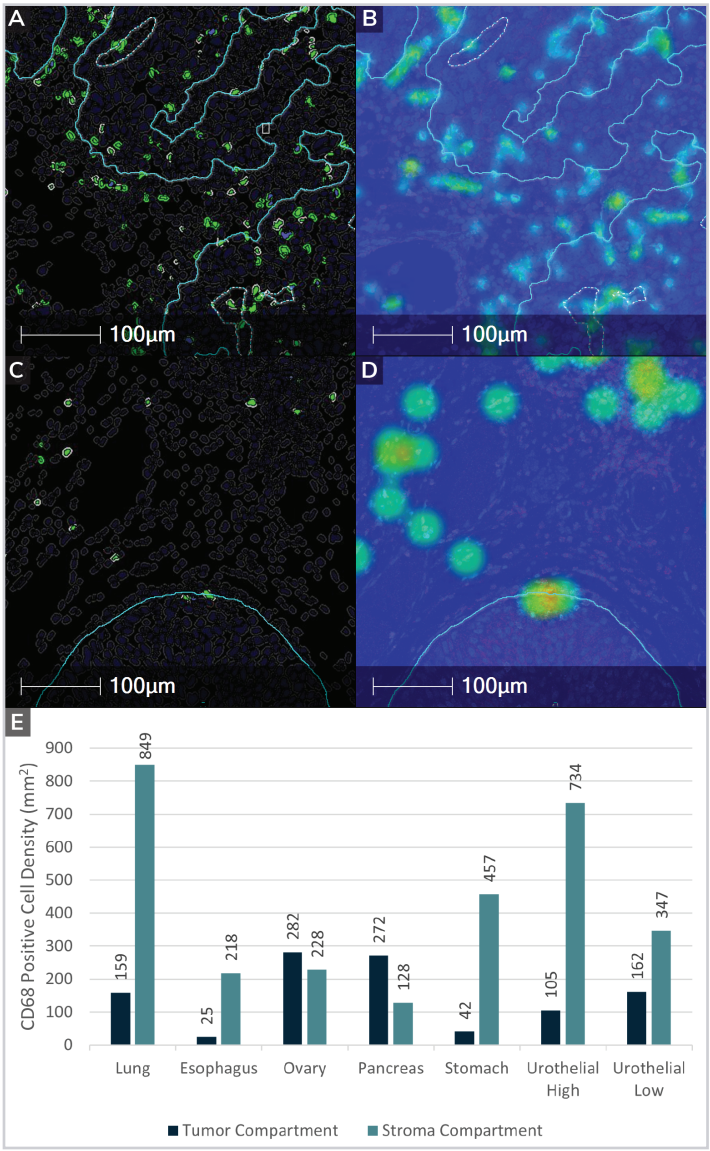

Figure 7. Macrophage density analysis. **A**. Cells with CD68 positive cytoplasm and/or nucleus (green) and tumor boundary (teal annotation) are shown in ovarian adenocarcinoma and **C** low-grade urothelial carcinoma. A density heatmap of CD68 positive cells in **B** ovarian adenocarcinoma and **D** low-grade urothelial carcinoma, with warmer (redder) colors correlating with increased cell density. **E**. Quantification of macrophage densities in tumoral and stromal compartments.

Infiltration Analysis of CD3+ cells

Next, the infiltration function of the Spatial Analysis module was used to quantify the spatial distribution of T cells within the TME, an important prognostic indicator and therapeutic target in cancer.[1] Highplex FL was used to define the positivity threshold for CD3, a biomarker commonly used to detect T cells due to its membrane expression on all mature T cells, and to identify all CD3+ T cells in the tissues. Tumor boundaries were automatically annotated using the previously described tissue classifier (**Figure 8A, D**) and the Spatial Analysis module was used to draw the infiltration margin, composed in this analysis of three 100 µm bands around tumor boundaries (**Figure 8B, E**), and to construct spatial plots depicting T-cell localization relative to the margin (**Figure 8C, F**).

CD3 positive cell density data for each of the 100 µm tumor margin bands is provided by the Spatial Analysis module and was compared across cancer types. As depicted in **Figure 9**, quantitative infiltration analysis elucidated diverse spatial distributions of T cells within the TME of the seven cancers studied.

Conclusions

TME composition is an important component in a patient's response to treatment, and subsequently their prognosis.[1] However, the TME presents numerous complications to analysis, including heterogenous tissue structure and diverse cellular components, requiring skillful annotation and often complex biomarker panels for robust analysis. Here, we demonstrate how the

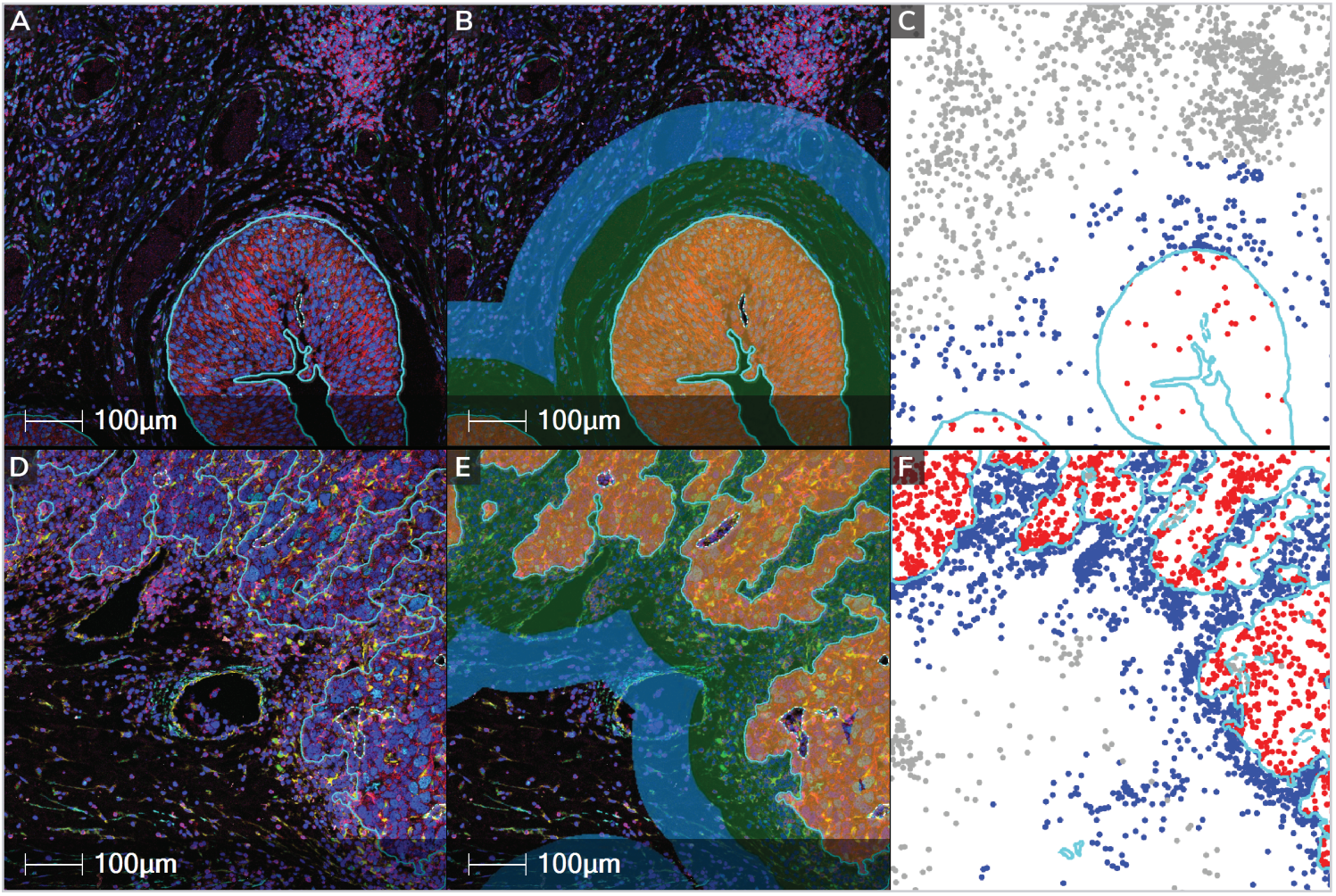

Figure 8. Analysis of T cell tumor infiltration. **A, B**. The tumor boundary (teal annotations) and infiltration margin bands (yellow, green, and blue colored bands) are shown on low-grade urothelial carcinoma and **D, E** ovarian adenocarcinoma. **C, F**. HALO Spatial Plots show CD3 positive cells in the inner margin (red) and outer margin (blue), and CD3 positive cells excluded from the analysis in grey.

combination of HALO and HALO AI image analysis platforms results in a straightforward workflow for sensitive quantitative analysis of the TME in hyperplex IMC images, at the single cell level across different tumor types. Additional applications of the tools and workflow described here hold promise for uncovering novel cellular dynamics that will inform our understanding of, and therapeutic responses toward cancer.

References

1. Fridman W, Zitvogel L, Sautès–Fridman C et al. The immune contexture in cancer prognosis and treatment. Nat Rev Clin Oncol **14**: 717–734 (2017). DOI: 10.1038/nrclinonc.2017.101.

2. Giesen C, Wang H, Schapiro D et al. Highly multiplexed imaging of tumor tissues with subcellular resolution by mass cytometry. Nat Methods **11**: 417-422 (2014). DOI: 10.1038/nmeth.2869.

3. Menz A, Gorbokon N, Viehweger F et al. Pan-keratin Immunostaining in Human Tumors: A Tissue Microarray Study of 15,940 Tumors. Int J Surg Pathol **0 (0)**: (2022). DOI: 10.1177/10668969221117243.

4. Brunnström H, Johansson A, Westbom-Fremer S et al. PD-L1 immunohistochemistry in clinical diagnostics of lung cancer: inter-pathologist variability is higher than assay variability. Mod Pathol **30 (10)**: 1411-1421 (2017). DOI: 10.1038/modpathol.2017.59.

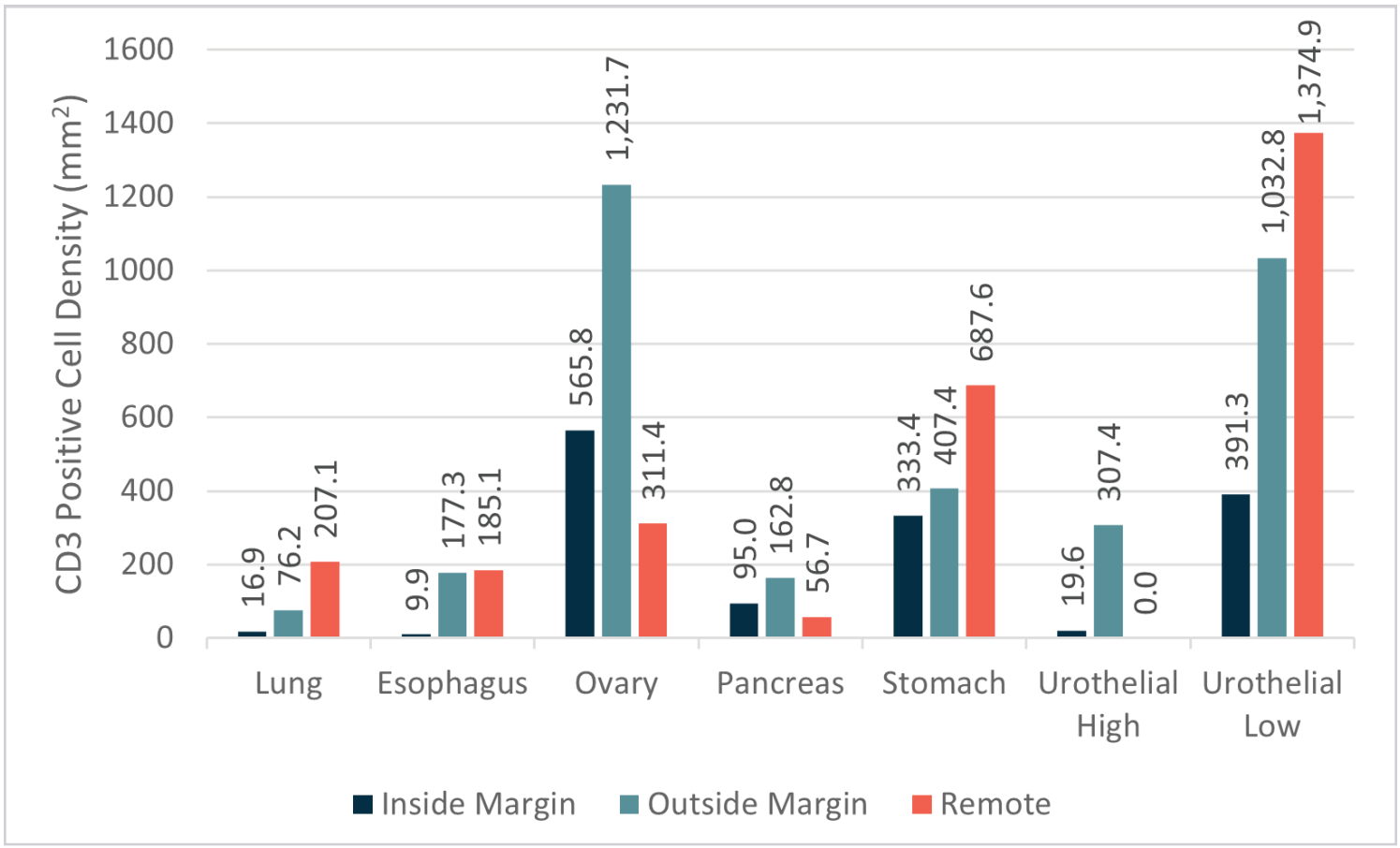

Figure 9. Quantification of T cell density. Positive cell density was measured 100 µm inside the tumor boundary in dark blue, and 100 µm and 200 µm outside the tumor boundary in teal and orange respectively across multiple cancer types.

5. Soo R, Lim J, Asuncion B et al. Determinants of variability of five programmed death ligand-1 immunohistochemistry assays in non-small cell lung cancer samples. Oncotarget **9 (6)**: 6841-6851 (2018). DOI: 10.18632/oncotarget.23827.

6. Van Seijen M, Brcic L, Gonzales A et al. Impact of delayed and prolonged fixation on the evaluation of immunohistochemical staining on lung carcinoma resection specimen. Virchows Arch **475**: 191-199 (2019). DOI: 10.1007/s00428-019-02595-9.

US Headquarters

Indica Labs, Inc
8700 Education Pl NW, Bldg B
Albuquerque, NM 87114 USA
+1 (505) 492-0979
info@indicalab.com

UK and Europe

+44 (0)1789 765 721
emea@indicalab.com

Japan

+81 (0)70 4180 7730
japan@indicalab.com

China

+86 13761896143
china@indicalab.com

Tech Support: support@indicalab.com
Website: https://indicalab.com

indica labs @Indica_Labs @IndicaLabs.HALO

HALO AI by indica labs